

# CrystEngComm

Accepted Manuscript



This is an *Accepted Manuscript*, which has been through the Royal Society of Chemistry peer review process and has been accepted for publication.

*Accepted Manuscripts* are published online shortly after acceptance, before technical editing, formatting and proof reading. Using this free service, authors can make their results available to the community, in citable form, before we publish the edited article. We will replace this *Accepted Manuscript* with the edited and formatted *Advance Article* as soon as it is available.

You can find more information about *Accepted Manuscripts* in the [Information for Authors](#).

Please note that technical editing may introduce minor changes to the text and/or graphics, which may alter content. The journal's standard [Terms & Conditions](#) and the [Ethical guidelines](#) still apply. In no event shall the Royal Society of Chemistry be held responsible for any errors or omissions in this *Accepted Manuscript* or any consequences arising from the use of any information it contains.

Cite this: DOI: 10.1039/c0xx00000x

[www.rsc.org/xxxxxx](http://www.rsc.org/xxxxxx)

# A Facile, One-pot Synthesis of Highly Branched Au Nanocorals and their enhanced electrocatalytic activity for Ethanol Oxidation

Zhenyuan Liu,<sup>‡</sup><sup>a</sup> Gengtao Fu,<sup>‡</sup><sup>a</sup> Yawen Tang,<sup>\*a</sup> Dongmei Sun,<sup>a</sup> Yu Chen,<sup>\*b</sup> and Tianhong Lu<sup>a</sup>*Received (in XXX, XXX) Xth XXXXXXXXXX 20XX, Accepted Xth XXXXXXXXXX 20XX*

DOI: 10.1039/b000000x

Gold nanocrystals (Au NCs) with particular three dimensional (3D) dendritic structure which usually possess special properties always attract considerable attention. Herein, a novel dendritic Au nanocorals was prepared by an effective and facile one-pot strategy with polyallylamine hydrochloride (PAH) as a capping agent and shape control agent, and ascorbic acid (AA) as a reductant. The formation mechanism was investigated by the time sequential evolution experiments, and the corals-like nanostructures originated from aggregation and growth mechanism. Additionally, the prepared Au nanocorals showed excellent electrocatalytic activity and stability for ethanol oxidation reaction (EOR), which could be attributed to the particular 3D dendritic structure and the great change in the electronic structure of the Au atom.

## Introduction

Shape-controlled synthesis of noble metal gold nanocrystals (Au NCs) has received extensive attention in recent years because of their shape-, size- and facet-dependent optical, electronic, sensing and catalytic properties.<sup>1-8</sup> For example, solution dispersible Au nanocube dimers with greatly enhanced two-photon luminescence and surface enhanced Raman scattering (SERS).<sup>7</sup> The trisoctahedral or concave cubic Au NCs have been demonstrated as effective and highly active electrocatalysts for methanol oxidation reaction (MOR) due to the presence of high-index facets on their surface.<sup>2</sup> Such Au NCs with well-defined morphologies are enclosed by the specific surface facets that are connected with their shapes, which have a profound influence on the catalytic property of NCs due to different facets have different surface atom arrangements (i.e., different surface energies). Therefore, the design and synthesis of unique Au nanostructures with well-controlled shape are critical for their application in catalysis.

To date, Au NCs with various shapes including dendrites,<sup>1, 6, 9-12</sup> flowers,<sup>13, 14</sup> rods,<sup>15, 16</sup> wires,<sup>17, 18</sup> concave cubes,<sup>2, 19</sup> trisoctahedra,<sup>20, 21</sup> and cubes,<sup>7</sup> have been synthesized by different methods such as wet chemical reduction, hydrothermal reduction, electro-deposition, seeded growth, and ionic liquid-assisted growth, etc. For example, wang and co-workers prepared the flower-shaped Au nanostructures through a wet chemical reduction with the assistance of gum Arabic molecules, which is quite unique in its simplicity and remarkably facilitates the synthetic procedure in comparison with commonly used seed-mediated growth approach.<sup>14</sup> Among them, the dendritic Au NCs with hyperbranched architectures are particularly interesting due

to their unique surface properties, such as their rough surface with low coordinated atoms (i.e., the atomic steps and kinks) and large surface area, which can endow the NCs with significantly enhanced catalytic activity through providing a large number of active sites for catalysis.<sup>1-6</sup> Meanwhile, the particular three dimensional (3D) dendritic structure is in favor of reactant transport and O<sub>2</sub> diffusion through the metal surface, thus enhancing the reaction kinetics. For instance, wang and co-workers prepared the single-crystalline dendritic Au nanostructures by electro-deposition method in the presence of ethylenediamine (EDA), exhibiting superior electrocatalytic activity toward ethanol oxidation reaction (EOR) in comparison with the polycrystalline Au NCs.<sup>1</sup> Similarly, Raj and co-workers reported a simple wet chemical method for the synthesis of nanostructured flower-like nanostructures using N-2-hydroxyethylpiperazine-N-2-ethanesulphonic acid (HEPES) as a reductant and stabilizing agent, and demonstrated the outstanding electrocatalytic activity toward the EOR and oxygen reduction reaction (ORR).<sup>9</sup> Despite those impressive advances in catalysis, the shape-controlled synthesis of dendritic Au NCs is still troubled by some issues such as complex reaction steps, low yield/purity, unsatisfactory uniformity, and failed to mass production.

Herein, we reported a facile, one-pot chemical reduction method for the high yield synthesis of 3D dendritic-like Au NCs with the assistance of polyallylamine hydrochloride (PAH), which look like the pint-sized “corals” structure (named as Au nanocorals). The as-prepared Au nanocorals showed enhanced electrocatalytic activity and stability for EOR compared to the polycrystalline Au NCs. The enhanced electrocatalytic activity

can be ascribed to the particular 3D dendritic structure and the great change in the electronic structure of the Au atom.

## Experimental

### Reagents and chemicals

Polyallylamine hydrochloride (PAH, weight-average molecular weight 150 000) was supplied by Nitto Boseki Co., Ltd (Tokyo, Japan). Hydrogen tetrachloroaurate (III) tetrahydrate ( $\text{HAuCl}_4 \cdot 4\text{H}_2\text{O}$ ) and ascorbic acid (AA) were purchased from Sinopharm Chemical Reagent Co., Ltd. (Shanghai, China). Other reagents were of analytical reagent grade and used without further purification. All the aqueous solutions were prepared with Millipore water having a resistivity of 18.2 M $\Omega$ . The solution pH was adjusted by the addition of dilute NaOH or HCl solution.

### Preparation of the Au nanocorals

In a typical synthesis, 1.0 mL of 0.01 M  $\text{HAuCl}_4$  and 0.4 mL of 0.5 M PAH (molarity of PAH given with respect to the repeating unit) were added into 8.0 mL deionized water with continuous stirring. After using a 0.1 M NaOH solution to adjust solution pH to 7.0, 0.5 mL of ascorbic acid (AA, 100 mg of 10 mL deionized water) was rapidly added into the mixture solution and mechanically stirred for 30 min at 40 °C. After the reaction, the obtained Au nanocorals were separated by centrifugation at 15 000 rpm for 10 min, washed several times with water, and then dried at 60 °C for 5 hours in a vacuum dryer. Finally, the Au nanocorals were treated with UV irradiation (wavelength at 185 and 254 nm in air for 4 h) to remove the capping agent (i.e., PAH) prior to electrochemical testing.

For comparison, the polycrystalline Au NCs prepared under the same conditions as Au nanocorals except for the exclusion of PAH.

### Physical characterizations

Scanning electron microscopy (SEM) images were taken on a JSM-2010 microscopy at an accelerating voltage of 20 kV. Transmission electron microscopy (TEM) measurements were made on a JEOL JEM-2100F transmission electron microscopy operated at an accelerating voltage of 200 kV. The samples were prepared by placing a drop of the colloidal solution or catalyst powder dispersion in ethanol solution (99%) on a carbon film coated Cu grid (3mm, 300 mesh), followed by drying under ambient conditions. Energy dispersive X-ray (EDX) analysis of particles was carried out on a JEOL JSM-7600F SEM. X-ray diffraction (XRD) patterns of nanocrystals were obtained with Model D/max-rC X-ray diffractometer using Cu K $\alpha$  radiation source ( $\lambda=1.5406$  Å) and operating at 40 kV and 100 mA. X-ray photoelectron spectroscopy (XPS) measurements were performed with a Thermo VG Scientific ESCALAB 250 spectrometer with a monochromatic Al K $\alpha$  X-ray source (1486.6 eV photons), and the vacuum in the analysis chamber was maintained at about  $10^{-9}$  mbar. The binding energy was calibrated by means of the C1s peak energy of 284.6 eV. The ultraviolet and visible spectroscopy (UV-vis) datas were recorded at room temperature on a Shimadzu UV3600 spectrophotometer equipped with 1.0 cm

quartz cells. Fourier transform infrared (FT-IR) was carried out using a Nicolet 520 SXFTIR spectrometer.

### Electrochemical instrument

All electrochemical experiments were performed using a CHI 660 C electrochemical analyzer (CH Instruments, Shanghai, Chenghua Co.). A standard three electrode system was used for all electrochemical experiments, which consisted of a Pt wire as the auxiliary electrode, a saturated calomel reference electrode (SCE) protected by Luggin capillary with KCl solution as the reference electrode, and a catalyst modified glassy carbon electrode as the working electrode. All potentials in this study were reported with respect to the SCE. All electrochemical measurements were carried out at 30 °C.

An evenly distributed suspension of catalyst was prepared by ultrasonating the mixture of 10 mg catalyst and 5 mL  $\text{H}_2\text{O}$  for 30 min. 12  $\mu\text{L}$  of the resulting suspension was laid on the surface of the pre-cleared glassy carbon electrode (5 mm diameter, 0.196  $\text{cm}^2$ ). After drying at room temperature, 2.5  $\mu\text{L}$  of Nafion solution (5 wt%) was layered on the surface of the modified electrode and allowed to dry. Thus, the working electrode was obtained, and the specific loading of the Au metal on the electrode surface was about 122.4  $\mu\text{g}\cdot\text{cm}^{-2}$ . Electrochemical measurements for ethanol oxidation were conducted in  $\text{N}_2$ -saturated 0.5 M NaOH solution with 1.0 M  $\text{CH}_3\text{CH}_2\text{OH}$ . Before electrocatalytic experiments, all working electrodes were pretreated by cycling the potential between 0 and 1.5 V for 50 cycles until a stable Cyclic voltammetry (CV) curve was obtained in order to remove any surface contamination prior to electrochemical testing. CV measurements were conducted in  $\text{N}_2$ -saturated 0.5 M  $\text{H}_2\text{SO}_4$  solution.

## Results and discussion

### Characterization of the as-prepared Au nanocorals

The structural features of the as-prepared Au NCs were firstly investigated by SEM (Fig. 1A). The nanocrystals seemingly have a three dimensional (3D), dendritic-like structure composed of a dozen or more branches, which is similar to pint-sized corals (the top-right inset in Fig. 1A). A further insight into the morphology of Au NCs was obtained from TEM images (Fig. 1B-C), confirming the highly branched coral-shaped Au nanostructure. From the magnified TEM image of an individual Au nanocoral (Fig. 1D), the dimensions of the branches can be estimated to be  $20 \pm 5$  nm in width and  $50 \pm 5$  nm in length. The corresponding selected area electron diffraction (SAED) pattern of the individual Au-NC displays discontinuous concentric rings, composed of bright discrete diffraction spots (inset in Fig. 1D), indicating the high crystallinity degree of the Au nanocorals. More structural information was also provided by HRTEM. The fringes with a lattice spacing of 0.240 nm are observed at most regions on the branch surface (Fig. 1E), close to the {111} lattice spacing of the face centered cubic (fcc) Au crystal (0.235 nm), demonstrating that Au nanocorals grown along the {111} direction. The corresponding fast Fourier transform (FFT) patterns indicate the single-crystalline nature of the branches

(inset in Fig. 1E). Such highly crystalline 3D dendritic-like Au nanostructure, consisting of interconnected Au branches, are believed to be a good candidate for electrocatalysts, owing to their unique surface properties, such as their rough surface with abundant corners and a large surface area available for accelerating the reaction.<sup>1, 6, 22, 23</sup>

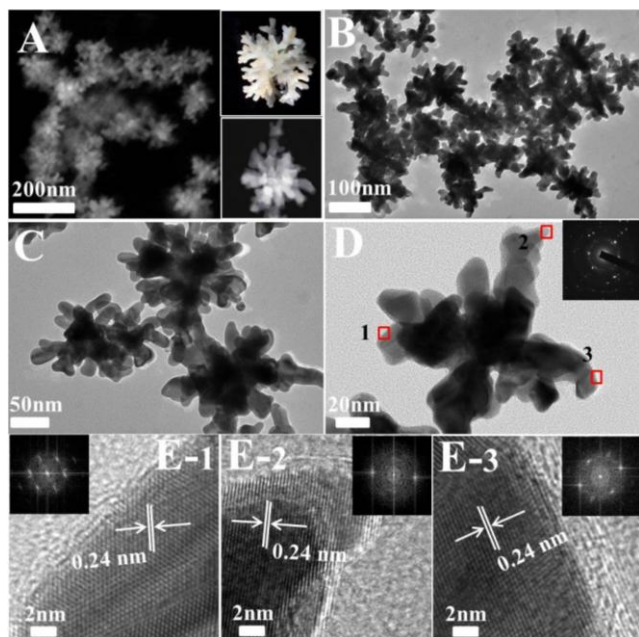


**Fig. 1** (A) Typical SEM image of the as-prepared Au nanocorals, the top-right and bottom-right insets in (A) are the corresponding ideal structure model and magnified SEM image of dendritic-like Au nanocorals, respectively. (B, C) Typical TEM images of the Au nanocorals. (D) TEM image of an individual Au nanocoral. (E) HRTEM images of the branches taken from regions 1, 2 and 3 marked by squares in (D), respectively (insets E1-3: FFT patterns from the corresponding areas).

To better understand the formation/growth process of coral-like Au NCs, the intermediate nanocrystals produced at different reaction durations are investigated by TEM (Fig. 2). At the initial stage of the reaction (30 s), the small-size nanoparticles with favorable dispersibility were formed from the fast reduction of Au<sup>III</sup> by AA (Fig. 2A). When the reaction time increase to 1 min, additional precursor reduction occurred in which Au atoms were grown tightly close to the initial seeds surface (Fig. 2B), resulting in growth of the branched Au nanoparticles. With an increase of reaction time (Fig. 2C and D), the Au particle size continued to increase, accompanying the branches gradually grow from the aggregate seeds. Careful observation of the TEM image from Fig. 2E, more and more branches were generated as the reaction proceeded to 30 min. When the reaction time is further extended to 60 min (Fig. 2F), no significant change is observed for the Au NCs in terms of both size and shape, is likely due to the complete consumption of Au<sup>III</sup> in the reaction system. Thus, the formation of such coral-like structures is likely ascribed to the nanocrystal aggregation and growth mechanism. The shape evolution of the Au NCs was also reflected in the color change of the reaction solution (Fig. 3). The color of the solution

changed from faint yellow to wathet blue, and finally to deep blue over the course of reaction, which corresponds to the sequential reduction of Au<sup>III</sup> and formation of coral-like nanostructures.

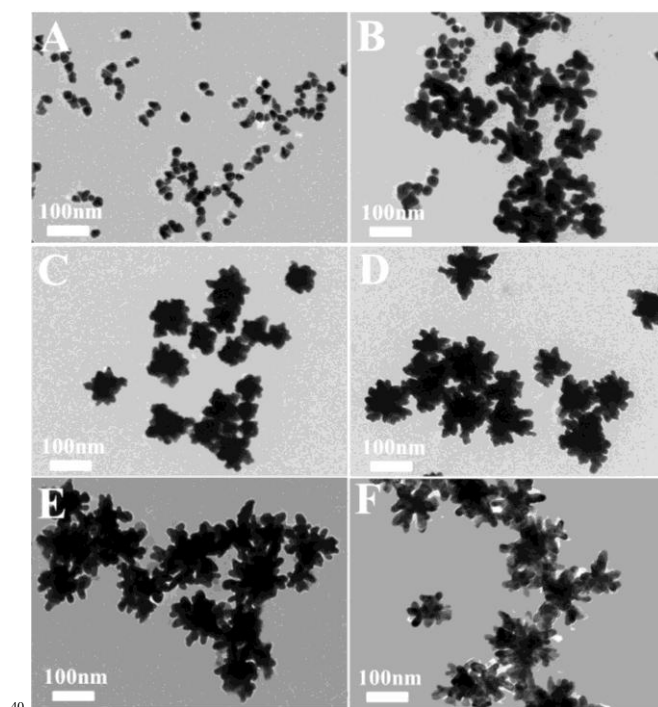


**Fig. 2** TEM images of the Au NCs collected at different growth stages: (A) 30 s, (B) 1 min, (C) 5 min, (D) 10 min, (E) 30 min, and (F) 60 min.

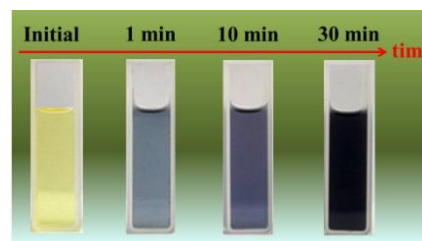


**Fig. 3** Digital photographs of the Au NCs at different growth stages.

The chemical composition and crystal structure of the as-prepared Au nanocorals were characterized by EDX spectrum and XRD pattern (Fig. 4). The EDX spectrum shows the characteristic peaks corresponding to the Au metal. The result demonstrates that the Au nanocorals only include Au element, revealing high purity of Au NCs. The XRD pattern of the products is identical to the Au crystal (JCPDS standard 04-0784), demonstrating that the as-prepared Au NCs possess a *fcc* structure (Fig. 4B). The sharp diffraction features indicate that the Au nanocorals possess highly crystalline. Meanwhile, the intensity ratio of (111) peak to (200) peak for the Au nanocorals is about 2.25, which is larger than those of the standard value calculated from Au JCPDS standard data (1.90). The result suggests that the {111} facets were the predominant growth orientation in the Au nanocorals, in consistent with the HRTEM characterization (Fig. 1E).

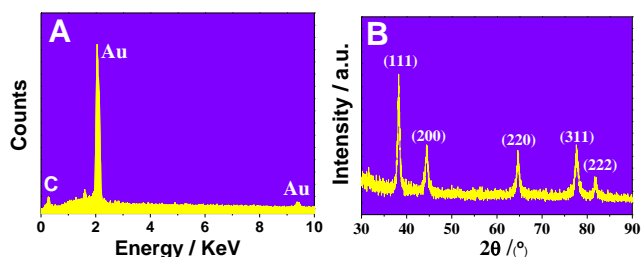


**Fig. 4** (A) EDX spectrum and (B) XRD pattern of the as-prepared Au nanocorals.

The electronic structure and element state of Au atoms in the Au nanocorals were qualitatively characterized by XPS. XPS measurement shows that the binding energy of Au 4f peaks ( $4f_{7/2} = 83.40$  eV,  $4f_{5/2} = 87.05$  eV) in the Au nanocorals are close to the standard values of bulk Au ( $4f_{7/2} = 83.80$  eV,  $4f_{5/2} = 87.45$  eV) metals (Fig. 5A), demonstrating that Au<sup>III</sup> precursors are successfully reduced in our synthesis. The slight negatively shift of binding energies (ca. 0.40 eV) may originate from interaction between PAH and Au nanocorals.<sup>24</sup> Meanwhile, the binding energy values of the Au 4f in the Au nanocorals also negatively shift by ca. 0.3 eV compared to that of the polycrystalline Au NCs obtained by the control experiment without PAH. As shown in Fig. 5B, the UV-vis spectra of HAuCl<sub>4</sub> obviously change after adding PAH solution, indicating that HAuCl<sub>4</sub> can interact with PAH to form PAH-Au<sup>III</sup> complexes (i.e. confirming a strong Au-N interaction). Specifically, N atom in PAH has a high electron density due to the lone pair electrons of -NH<sub>2</sub> groups, and hence Au atoms withdraw electrons from the neighboring N atoms in PAH. FT-IR spectrum of the Au nanocorals is similar to that of pure PAH (Fig. 5C), showing the Au nanocorals are covered with PAH molecules. The binding of PAH on Au nanocorals surface was visualized by EDX mapping (Fig. 5D). The N element mapping pattern is identical with Au element mapping pattern, indicating the uniform distribution of PAH on the Au nanocorals surface. Due to the strong Au-N interaction between Au<sup>0</sup> and PAH, the binding of PAH on Au nanocorals surface is responsible for the shift of Au binding energy.

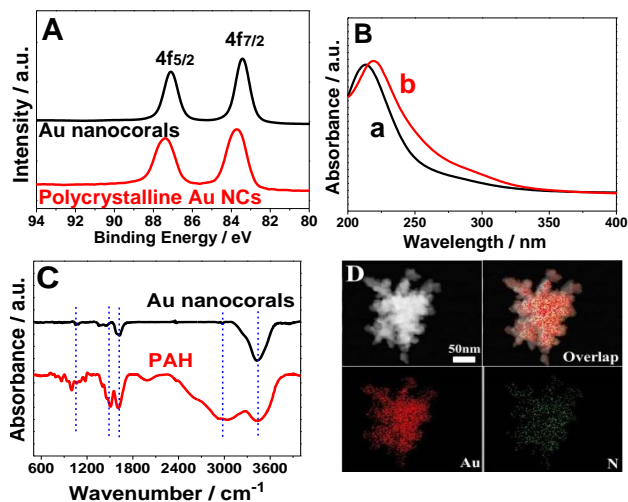


**Fig. 5** (A) XPS spectra for Au 4f region of the Au nanocorals and polycrystalline Au NCs. (B) UV-vis absorption spectra of (a) HAuCl<sub>4</sub> solution, and (b) the mixture solution of PAH and

HAuCl<sub>4</sub> (the molar ratio of PAH monomer to HAuCl<sub>4</sub> is 20:1). (C) FT-IR spectra of as-prepared Au nanocorals and pure PAH. (D) EDS elemental mapping images of Au and N in the Au nanocorals.

Additionally, PAH also play an important role in obtaining well-defined and homo-dispersive Au nanocorals. In the absence of PAH, irregular and random aggregation polycrystalline Au NCs instead of coral-like Au NCs are obtained (Fig. 6). Consequently, PAH also can serve as a shape control agent and capping agent to effectively prevent the aggregation of nanocrystals because of their bulky molecule size, excellent hydrophilic property and positively charged polyelectrolytic nature of PAH molecules,<sup>25-33</sup> which contribute to the excellent dispersity and specific shape of Au nanocorals.

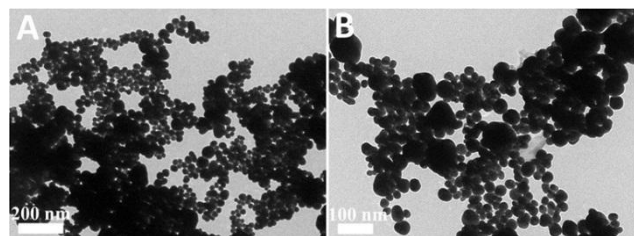


**Fig. 6** TEM images of the product prepared under the same conditions as in Fig. 1 except for the exclusion of PAH.

#### Electrochemical test

The electrochemical properties of the Au nanocorals were firstly investigated by cyclic voltammetry (CV) in N<sub>2</sub>-saturated 0.5 M H<sub>2</sub>SO<sub>4</sub> solution (Fig. 7A). The polycrystalline Au NCs prepared under the identical conditions in the absence of PAH used as references for comparison. The electrochemically active surface area (ECSA) of Au NCs were calculated from CVs in 0.5 M H<sub>2</sub>SO<sub>4</sub> solution by integrating the reduction charge of Au oxide layer and assuming a value of 400  $\mu\text{C cm}^{-2}$  for the reduction charge of a Au oxide monolayer on the Au surface.<sup>9, 34, 35</sup> The ECSA of Au nanocorals ( $11.3 \text{ m}^2 \text{ g}^{-1}$ ) is much larger than that of the polycrystalline Au NCs ( $5.1 \text{ m}^2 \text{ g}^{-1}$ ), which is most likely due to unique 3D dendritic-like structure. Fig. 7B depicts the specific activity of the two different catalysts recorded in a mixture of 0.5 M NaOH + 1.0 M CH<sub>3</sub>CH<sub>2</sub>OH solution (the current densities were normalized with reference to ECSA values of catalysts). The positive anodic peak current density of ethanol on Au nanocorals ( $1.5 \text{ mA cm}^{-2}$ ) is 2.5 times higher than that on the polycrystalline Au NCs ( $0.6 \text{ mA cm}^{-2}$ ), suggesting that the particular dendritic morphology of the Au nanocorals improves the electrocatalytic activity of Au nanoparticles for ethanol oxidation. Furthermore, at  $0.20 \text{ mA cm}^{-2}$ , the oxidation potential of ethanol on Au nanocorals shifts negatively ca. 80 mV compared to the polycrystalline Au NCs, illustrating that Au nanocorals have the lower onset potential. The higher ethanol oxidation current and the lower onset potential indicate that the Au nanocorals have much better electrocatalytic activity compared to that of the polycrystalline Au NCs.

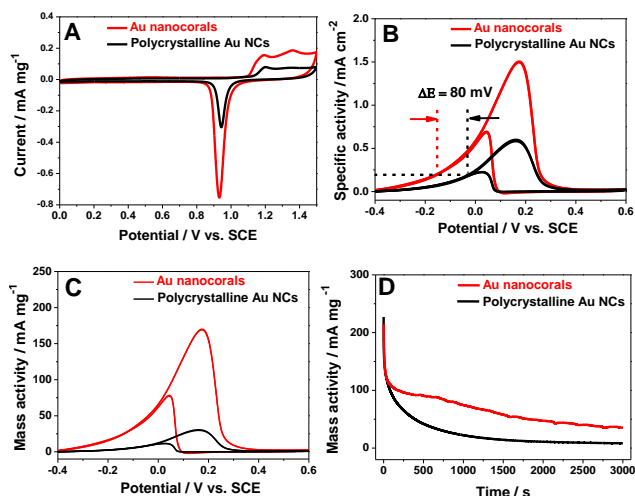


**Fig. 7** (A) CV curves for Au nanocorals and polycrystalline Au NCs in  $N_2$ -saturated 0.5 M  $H_2SO_4$  solution at a scan rate of 50  $mV s^{-1}$ . CV curves for Au nanocorals and polycrystalline Au NCs in  $N_2$ -saturated 0.5 M NaOH + 1.0 M  $CH_3CH_2OH$  solution at a scan rate of 50  $mV s^{-1}$ , which are normalized to (B) the ECSA (specific activity) and (C) Au mass (mass activity), respectively. (D) Chronoamperometry curves for Au nanocorals and polycrystalline Au NCs in  $N_2$ -saturated 0.5 M NaOH + 1.0 M  $CH_3CH_2OH$  solution for 3000 s at 0.17 V potential.

The mass activities of Au nanocorals and polycrystalline Au NCs for EOR were also investigated by CV. The ethanol oxidation peak current density on Au nanocorals is 5.3 times higher than that on the polycrystalline Au NCs (Fig. 7C), further indicating Au nanocorals hold promise as potentially practical electrocatalysts for the EOR. The improved activity of Au nanocorals most likely originate from the following reasons: (i) The particular 3D dendritic structure provides high ECSA, and facilitates reactant effective transport and  $O_2$  diffusion; (ii) The abundant corners, which including many high-density atomic steps, terraces and defect atoms, exposed on the dendritic surface can effectively serve as catalytically active sites; (iii) According to the XPS results (Fig. 5A), the Au 4f<sub>7/2</sub> and Au 4f<sub>5/2</sub> signal of Au nanocorals was ca. 0.40 eV and 0.30 eV lower than those of the standard values of bulk Au and polycrystalline Au NCs, respectively, indicating that the Au surface in the Au nanocorals is in electron-rich environments. The increased electron density of Au would be beneficial to ethanol activation due to an enhanced electron donation from Au to the  $\pi^*$  orbital of the surface intermediates, which would also account for the higher intrinsic catalytic activity of Au nanocorals than the reference polycrystalline Au NCs. In addition, the long term catalytic stability for EOR was confirmed by chronoamperometric experiments at 0.6 V for 3000 s. As observed in Fig. 7D, the current intensity decay of the Au nanocorals is much lower than those of the polycrystalline Au NCs during the entire time range, thus indicating that the Au nanocorals are more stable as an electrocatalyst for EOR. The particular interconnected 3D structure suppresses Ostwald ripening effect<sup>36, 37</sup> that restrain electrochemical corrosion/dissolution of Au nanoparticles at high

potential are responsible for the enhanced durability of the Au nanocorals.

## Conclusions

In summary, this work presented a successful synthesis of 3D dendritic-like Au nanocorals via a facile one-pot chemical reduction method in the presence of PAH. Herein, PAH is used efficiently as a complex-forming agent, capping agent, and shape control agent. Through the time sequential evolution experiments, the formation of such coral-like structures is likely ascribed to the nanocrystal aggregation and growth mechanism. The prepared Au nanocorals showed excellent catalytic performance for EOR, which can be attributed to the particular 3D dendritic structure and the great change in the electronic structure of the Au atom.

## Acknowledgments

This work was supported by NSFC (21376122 and 21273116), Natural Science Foundation of Jiangsu Province (BK20131395), the United Fund of NSFC and Yunnan Province (U1137602), Industry-Academia Cooperation Innovation Fund Project of Jiangsu Province (BY2012001), and a project funded by the Priority Academic Program Development of Jiangsu Higher Education Institutions. Fundamental Research Funds for the Central Universities (GK201402016), and the Starting Funds of Shaanxi Normal University.

## Notes and references

- <sup>a</sup> Jiangsu Key Laboratory of New Power Batteries, Jiangsu Collaborative Innovation Centre of Biomedical Functional Materials, School of Chemistry and Materials Science, Nanjing Normal University, Nanjing 210023, China  
<sup>b</sup> School of Materials Science and Engineering, Shaanxi Normal University, Xi'an 710062, China  
 Fax: 86-25-83243286; Tel: +86-25-85891651;  
 E-mail: tangyawen@njnu.edu.cn (Y. W. Tang)  
 ndchenyu@gmail.com (Y. Chen)

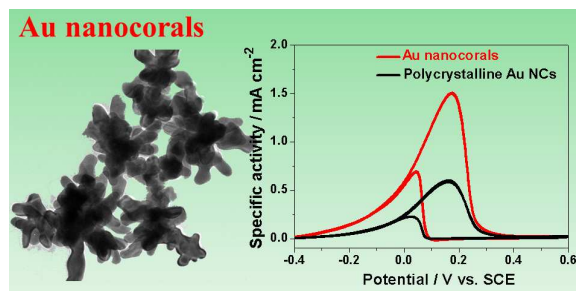
‡ These two authors made an equal contribution to this work

- J. J. Feng, A. Q. Li, Z. Lei and A. J. Wang, *ACS Appl. Mater. Interfaces*, 2012, **4**, 2570-2576.
- J. Zhang, H. Xia, C. Feng, C. Xi, D. Wang and X. Tao, *Langmuir*, 2014, **9**, 2480-2489.
- Y. Jin, Q. Li, G. Li, M. Chen, J. Liu, Y. Zou, K. Jiang and S. Fan, *Nanoscale Res. Lett.*, 2014, **9**, 1-6.
- I. Yoon, T. Kang, W. Choi, J. Kim, Y. Yoo, S. W. Joo, Q.-H. Park, H. Ihee and B. Kim, *J. Am. Chem. Soc.*, 2008, **131**, 758-762.
- F. Behafarid, J. Matos, S. Hong, L. Zhang, T. S. Rahman and B. Roldan Cuenya, *ACS nano*, 2014, DOI: 10.1021/nn406568b.
- T. H. Lin, C. W. Lin, H. H. Liu, J. T. Sheu and W.-H. Hung, *Chem. Commun.*, 2011, **47**, 2044-2046.
- X. L. Liu, S. Liang, F. Nan, Z. J. Yang, X. F. Yu, L. Zhou, Z. H. Hao and Q. Q. Wang, *Nanoscale*, 2013, **5**, 5368-5374.
- Y. Yamauchi, L. Wang, H. Atae-Esfahani, N. Fukata, T. Nagaura and S. Inoue, *J. Nanosci. Nanotechnol.*, 2010, **10**, 4384-4387.
- B. K. Jena and C. R. Raj, *Langmuir*, 2007, **23**, 4064-4070.
- G. Paneru and B. N. Flanders, *Nanoscale*, 2014, **6**, 833-841.

11. Y. Qin, Y. Song, N. Sun, N. Zhao, M. Li and L. Qi, *Chem. mater.*, 2008, **20**, 3965-3972.
12. X. L. Tang, P. Jiang, G. L. Ge, M. Tsuji, S. S. Xie and Y. J. Guo, *Langmuir*, 2008, **24**, 1763-1768.
13. L. Wang, M. Imura and Y. Yamauchi, *CrystEngComm*, 2012, **14**, 7594-7599.
14. L. Wang, C. H. Liu, Y. Nemoto, N. Fukata, K. C. W. Wu and Y. Yamauchi, *Rsc Adv.*, 2012, **2**, 4608-4611.
15. N. Garg, C. Scholl, A. Mohanty and R. Jin, *Langmuir*, 2010, **26**, 10271-10276.
16. X. Ye, Y. Gao, J. Chen, D. C. Reifsnnyder, C. Zheng and C. B. Murray, *Nano Lett.*, 2013, **13**, 2163-2171.
17. J. Xu, H. Wang, C. Liu, Y. Yang, T. Chen, Y. Wang, F. Wang, X. Liu, B. Xing and H. Chen, *J. Am. Chem. Soc.*, 2010, **132**, 11920-11922.
18. Y. Imura, S. Hojo, C. Morita and T. Kawai, *Langmuir*, 2014, **30**, 1888-1892.
19. J. Zhang, M. R. Langille, M. L. Personick, K. Zhang, S. Li and C. A. Mirkin, *J. Am. Chem. Soc.*, 2010, **132**, 14012-14014.
20. X. L. Zhong and Z. Y. Li, *Adv. Mater. Res.*, 2012, **1**, 1-12.
21. Y. Yu, Q. Zhang, X. Lu and J. Y. Lee, *J. Phys. Chem. C*, 2010, **114**, 11119-11126.
22. X. J. Liu, C. H. Cui, M. Gong, H. H. Li, Y. Xue, F. J. Fan and S. H. Yu, *Chem. Commun.*, 2013, **49**, 8704-8706.
23. B. Lim, M. Jiang, P. H. Camargo, E. C. Cho, J. Tao, X. Lu, Y. Zhu and Y. Xia, *Science*, 2009, **324**, 1302-1305.
24. G. Fu, L. Ding, Y. Chen, J. Lin, Y. Tang and T. Lu, *CrystEngComm*, 2014, **16**, 1606-1610.
25. G. Fu, W. Han, L. Yao, J. Lin, S. Wei, Y. Chen, Y. Tang, Y. Zhou, T. Lu and X. Xia, *J. Mater. Chem.*, 2012, **22**, 17604-17611.
26. G. Fu, X. Jiang, L. Ding, L. Tao, Y. Chen, Y. Tang, Y. Zhou, S. Wei, J. Lin and T. Lu, *Appl. Catal. B: Environ.*, 2013, **138-139**, 167-174.
27. G. Fu, X. Jiang, M. Gong, Y. Chen, Y. Tang, J. Lin and T. Lu, *Nanoscale*, 2014, DOI: 10.1039/c4nr00947a.
28. G. Fu, X. Jiang, L. Tao, Y. Chen, J. Lin, Y. Zhou, Y. Tang and T. Lu, *Langmuir*, 2013, **29**, 4413-4420.
29. G. Fu, Z. Liu, Y. Chen, J. Lin, Y. Tang and T. Lu, *Nano Res.*, 2014, DOI: 10.1007/s12274-014-0483-2.
30. G. Fu, L. Tao, M. Zhang, Y. Chen, Y. Tang, J. Lin and T. Lu, *Nanoscale*, 2013, **5**, 8007-8014.
31. G. Fu, K. Wu, X. Jiang, L. Tao, Y. Chen, J. Lin, Y. Zhou, S. Wei, Y. Tang, T. Lu and X. Xia, *Phys. Chem. Chem. Phys.*, 2013, **15**, 3793-3802.
32. G. Fu, K. Wu, J. Lin, Y. Tang, Y. Chen, Y. Zhou and T. Lu, *J. Phys. Chem. C*, 2013, **117**, 9826-9834.
33. G. Fu, R. Zhao, L. Ding, L. Tao, J. Lin, Y. Chen, Y. Tang, Y. Zhou and T. Lu, *ChemPlusChem*, 2013, **78**, 623-627.
34. E. Higuchi, K. Hayashi, M. Chiku and H. Inoue, *Electrocatal.*, 2012, **3**, 274-283.
35. D. F. Yancey, E. V. Carino and R. M. Crooks, *J. Am. Chem. Soc.*, 2010, **132**, 10988-10989.
36. S. H. Sun, G. X. Zhang, D. S. Geng, Y. G. Chen, R. Y. Li, M. Cai and X. L. Sun, *Angew. Chem. Int. Edit.*, 2011, **50**, 422-426.
37. B. Y. Xia, W. T. Ng, H. Bin Wu, X. Wang and X. W. Lou, *Angew. Chem. Int. Edit.*, 2012, **51**, 7213-7216.

55

## Graphic abstract



Dendritic Au nanocorals was prepared by a facile one-pot strategy, exhibiting excellent catalytic activity and stability for ethanol oxidation reaction.